An experimental study of I beam-RHS column demountable joints with welded studs

Miguel A. Serrano-López*[1], Carlos López-Colina[1], Yong C. Wang [2], Miguel Lozano[1], Ismael García[1] and Fernando L. Gayarre[1]

[1] University of Oviedo, Dep. Construction and Manufacturing Engineering, Campus Gijón, 33203 Spain
[2] The University of Manchester, School of Mechanical, Aerospace and Civil Engineering, Manchester M13 9PL, United Kingdom

Abstract

This paper presents the results of an extensive experimental investigation on the behaviour of a new type of joint between open structural steel beam and rectangular hollow section (RHS) column. The proposed joint is demountable: threaded studs are welded to the front face of the hollow section column and angle cleat legs are then bolted to the column by means of the welded studs and to the beam flanges by ordinary bolts. Twenty-one full-scale single side or double side bolted beam-column joints combining different sections have been tested under monotonic and cyclic loads. The test results confirm that these joints behave as semi rigid and partial strength ones which possess sufficient stiffness and moment resistance for use in the construction of low to medium-rise steel buildings as an alternative to other traditional solutions. The proposed joints also exhibit a moderate energy dissipation capacity under cyclic loads, suitable for construction in moderate seismic regions. This research work demonstrates that the proposed joint is easy to execute on site without specialized manpower or expensive facilities.

Keywords: Tubular structures; Welded studs; Bolted connections; Joint characterization, Demountable construction; Cyclic behaviour.

1. Introduction

Traditionally, in steel building construction, open I or H profiles are used as beams and columns. In recent years there is a trend to use structural hollow sections as columns because they possess advantages in mechanical strength, fire resistance, maintenance costs, aesthetics and the possibility to create concrete filled composite columns for better utilization of space [1-2]. When using hollow sections as columns, a critical issue is cost-effective fabrication of the beam-column joints. Without access from inside the steel tube, direct bolting to the steel tube using ordinary bolts is not possible. Blind bolts such as flow-drill bolts are time-consuming and have limited resistance and therefore their applications in steel tubular construction are very rare [3-5]. Therefore, the common practice of making simple joints to tubular sections is to weld steel fin plate to the steel tube. However, this practice is still costly

* Corresponding author. Tel.: +34-985181947
E-mail address: serrano@uniovi.es (Miguel A. Serrano-López).

for fabrication and the resulting joints have limited stiffness and resistance. To improve welded joint stiffness and resistance, the reverse channel connection using standard bolts [6-7] may be considered, although this further increases the fabrication cost. Another alternative to achieve improved bending stiffness and moment resistance is direct welding of the steel open section beam to the steel tube [8], although this is again an expensive practice, even though it is possible to not weld the web of the steel beam.

This research proposes an alternative method of making joints to tubular sections, which combines the advantages of bolting (for easy construction) and welding (to avoid the problem of lack of access from inside the steel tube). In this method, threaded steel studs are welded to the face of the steel tube. Compared to welding a steel fin plate, welding steel studs is much easy as commonly done for composite beams. This makes it possible to construct the beam-column connection by bolting but the welded steel studs no longer require any access on the tube side for bolting. Furthermore, this connection system is demountable, making it possible to reclaim the steel members when the building reaches its end of service life. In fact, there have been some early attempts to use welded studs to make joints to tubular sections [9-10]. However, they were focussed on end-plate connections. It would be very difficult to execute steel structures with beam-column joints using end-plates and welded studs because of the difficulty of positioning a beam with two end plates between the corresponding tubular columns with the protruding welded steel studs on the tube walls. This problem associated with end-plate connection can be avoided by bolting top and seat angles as proposed in this paper.

Because this is a new type of connection, it is important to develop thorough understanding of the joint behaviour. In particular, this joint has the potential to develop considerable stiffness and bending moment resistance to achieve savings in overall structure design by exploring semi-rigid partial-strength design [11-13]. The current component based design method for joints in EC3 [14] is generally suitable for the proposed type of new joint, and previous research studies in [15-16] have provided some data to quantify the load-displacement behaviour of some components of the proposed joint, but it is necessary to provide experimental data to validate this method.

Although previous research studies regarding welded studs have investigated the static behaviour of shear connectors in steel bridges as in [17] or in steel composite beams [18], and fatigue resistance of shear studs [19-20], there is no experimental investigation of the cyclic behaviour of the proposed new joint.

Therefore, an extensive experimental campaign has been conducted to investigate the behaviour of full scale bolted beam-column joints with threaded welded steel studs, subjected to both monotonic and cyclic loads. The main aim of this program is to demonstrate that the proposed joint behaves as semi-rigid and partial-strength, and has a good level of energy absorption under cyclic loading for low to midrise building applications in moderately seismic

zones. This paper also demonstrates the ease with which the new proposed joint can be fabricated.

2. Experimental program

The experimental program included mechanical property tests and full scale joint tests. Standard tensile tests were carried out to obtain the mechanical properties of steel for the beams, columns and angle cleats that formed the beam-column joints. Tensile tests were also performed on the threaded studs to determine their mechanical characteristics.

2.1. General set-up of beam-column joint tests

A total of twenty-one full-scale beam-column joint tests were carried out and Table 1 summarises the main specimen parameters.

Table 1: Main dimensions of all beam-column joints

Specimen	Column	Beam	β ratio	Beam length L_B [mm]	Bolts M16	Studs
DMS1	SHS200.8	HEB200	1.0	457.4	8.8	M16×35 4.8
DMS2	SHS200.6	IPE300	0.75	457.3	8.8	M16×35 4.8
DMS3	SHS200.8	IPE300	0.75	457.4	8.8	M16×35 4.8
DMS4	RHS200.150.8	IPE300	1.0	457.5	8.8	M16×35 4.8
SMS1	SHS200.6	HEB200	1.0	786.7	10.9	M16×40 K800
SMS2	SHS200.8	HEB200	1.0	789.1	10.9	M16×40 K800
SMS3	SHS200.10	HEB200	1.0	787.2	10.9	M16×40 K800
SMS4	SHS200.6	IPE300	0.75	786.6	10.9	M16×40 K800
SMS5	SHS200.8	IPE300	0.75	789.2	10.9	M16×40 K800
SMS6	SHS200.10	IPE300	0.75	786.8	10.9	M16×40 K800
SMS7	RHS200.150.6	IPE300	1.0	793.4	10.9	M16×40 K800
SMS8	RHS200.150.8	IPE300	1.0	795.2	10.9	M16×40 K800
SMS9	RHS200.150.10	IPE300	1.0	794.5	10.9	M16×40 K800
SCS1	SHS200.6	HEB200	1.0	786.0	10.9	M20×40 4.8
SCS2	SHS200.8	HEB200	1.0	786.0	10.9	M20×40 4.8
SCS3	SHS200.10	HEB200	1.0	786.0	10.9	M20×40 4.8
SCS4	SHS200.6	IPE300	0.75	786.0	10.9	M20×40 4.8
SCS5	SHS200.8	IPE300	0.75	786.0	10.9	M20×40 4.8
SCS6	SHS200.10	IPE300	0.75	786.0	10.9	M20×40 4.8
SCS7	RHS200.150.6	IPE300	1.0	786.0	10.9	M20×40 4.8
SCS9	RHS200.150.10	IPE300	1.0	786.0	10.9	M20×40 4.8

Of these tests, seventeen were on one-sided joint as shown in Figure 1d and four tests were symmetrical with joints on both sides of the column as shown in Figure 1c.

The beams were either HEB200 or IPE300, representing wide or narrow flange open sections. The columns were either square hollow section SHS200mm or rectangular hollow section RHS200x150mm. The nominal length of the columns was 900mm. The beam was joined at the flanges to the column by bolting a pair non-symmetrical angle cleats LD120x80x10. The long legs of the angle cleats were bolted with four ordinary bolts to the top and the bottom flanges of the beam as shown in Figure 1(c). The short leg of each angle cleat was connected

to the column face by means of two welded threaded studs. The length of the angle cleats was equal to the corresponding beam flange width. There was no connection to the web of the beam because of the potential difficulty of execution on site to place the beam for connection on the web. This fabrication process makes it simple for site construction, but raises a concern about how the connected beam would develop sufficient shear resistance because it is commonly assumed that the web of the beam resists shear. However, a previous research study by the authors on welded connections between open section beams and tubular columns without welding the web [8] suggested that the flanges and their connections were able to develop sufficient shear resistance. This research will examine whether the same conclusion can be reached by using angle cleats to only the beam flanges.

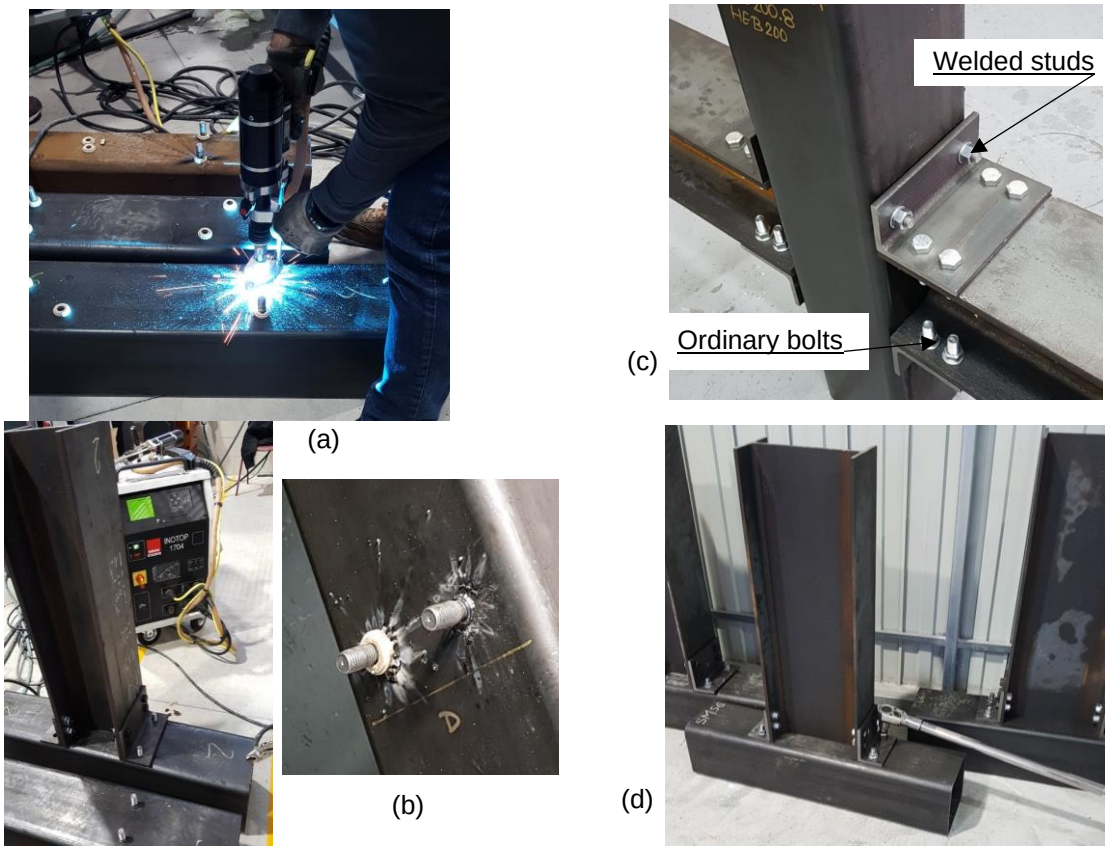

Figure 1: Preparation of specimens. (a) Welder gun. (b) Welded studs. (c) Double side joint. (d) Single side

The stud welding process was very easy. The studs were welded using a portable welding machine (model INOTOP 1704, made by Köster &-Co.). The welder gun was model Electronic KE 30 (Köster &-Co) as shown in figure 1(a). Figure 1(b) shows quality of the welding in detail. Figures 1(c) and 1(d) show respectively a double sided and a single sided joint during the tightening process. The studs would be welded in the fabrication shop with the steel tube in the horizontal position.

On the construction site, the joint would be easily made by first bolting the angle cleats to the column and then to the beam. Because there is no connection to the web of the beam, the beam can be placed horizontally without any obstruction.

Figure 2 shows the positions of holes in the angle cleat. The length of the angle cleat was 150 or 200 mm depending on the width of the beam section (IPE300 or HEB200) and the distance between the holes in the angle cleat (90 or 140 mm) varied accordingly.

A total of twenty one full-scale beam-column joints were tested, consisting of four double-sided joints (DMS1 to DMS4) and nine single-sided joints (SMS1 to SMS9) under monotonic load, and single-sided joints (SCS1 to SCS9) under cyclic load. In all tests, a servo-controlled hydraulic actuator (Ibertest GIB 500-MD2W) was attached to the reaction frame to apply the axial compression or axial tension load, with a maximum load capacity of 500 kN and a maximum stroke of 200 mm, operating under a displacement-controlled mode.

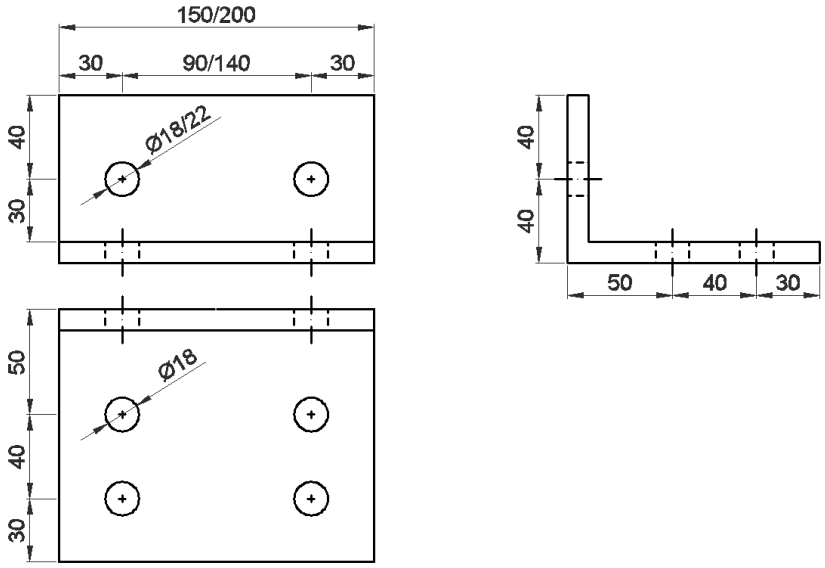

Figure 2: Hole positions in angle cleat

A DIC (digital image correlation) equipment Aramis model 5M (GOM) was used to measure deformations in all the tests by means of high resolution images obtained from the specimen surfaces during the tests. It is a non-contact and material independent measuring system that provides accurate 3D surface coordinates, 3D displacements, surface strain values and strain rates. This equipment can be synchronized with the actuator recording the applied load in real-time. The recorded data of load and displacements at many points of the specimen surface can be used to plot stress-strain curves in the characterization tests or to obtain moment - rotation curves of the joints, as will later be explained.

2.1.1. Set-up of monotonic tests

For the symmetric double sided joints tested under monotonic load (DMS), a vertical downwards displacement on top of the column was introduced while the ends of the beams were simply supported sitting on rollers as can be seen in figure 3(a). In case of single sided joints tested under monotonic load (SMS), a vertical downwards displacement was applied on the top of the upper flange of the I beam in the free end section of the cantilever. The horizontal movements of the column were prevented at the upper and lower ends by means of four threaded rods of 20 mm in diameter fixed to the reaction frame as shown in figure 3(b). Figure 3(c) shows a sketch with the elevation and plan view of these test arrangements, indicating their overall dimensions and boundary conditions. The speed of displacement of the actuator during the displacement-controlled tests was 4 mm/min.

(a)

(b)

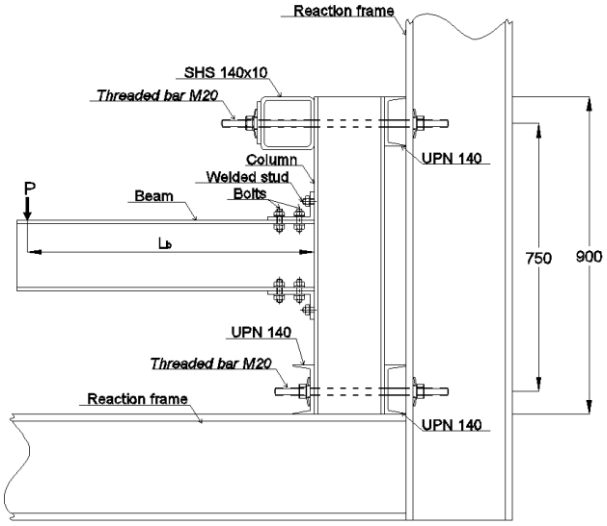

Elevation

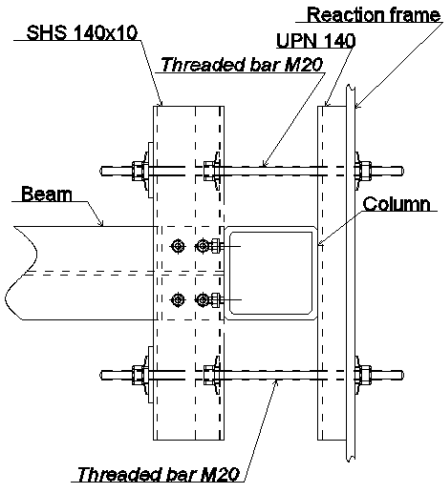

Plan view

(c)

Figure 3: General set-up of tests for joints. (a) Double sided specimen (DMS4). (b) Single sided specimen (SMS3) (c) Sketch of the horizontal restrain system.

2.1.2. Set-up of cyclic tests

Eight of the nine single-sided specimens tested under monotonic load were replicated and tested under cyclic loading. Since both compression and tension loads should be applied, a specific loading mechanism was purposed built as shown in figure 4a. It includes a pair of connecting rods that rotate on two pins. This mechanism allowed large rotations to occur in the joint while maintaining verticality of the hydraulic jack. Depending on the beam depth, some shim plates (see figure 4a) of different thicknesses were used to ensure availability of most of the jack displacement range. The vertical rods helped to reduce relative movements of the horizontal beams of the reaction frame when applying high compression loads. In addition, an outside bracing system with tensioned cables (see figure 4b) was used to minimise frame movements when applying a tension load by the actuator.

The tubular column was fixed to the frame by horizontal rods on both the top and bottom of the reaction frame in order to prevent horizontal displacements. Additionally, to prevent vertical movement of the column, four additional large rods of 20 mm in diameter inside the tube in the longitudinal direction, were firmly tightened to the reaction frame at the bottom and to a thick plate at the top of the column section. Figure 4(c) shows a sketch of these test arrangement indicating their overall dimensions and boundary conditions. This combination of horizontal and vertical rods ensured that no horizontal and vertical movement occurred at the column ends during the tests, as intended.

(a)

(b)

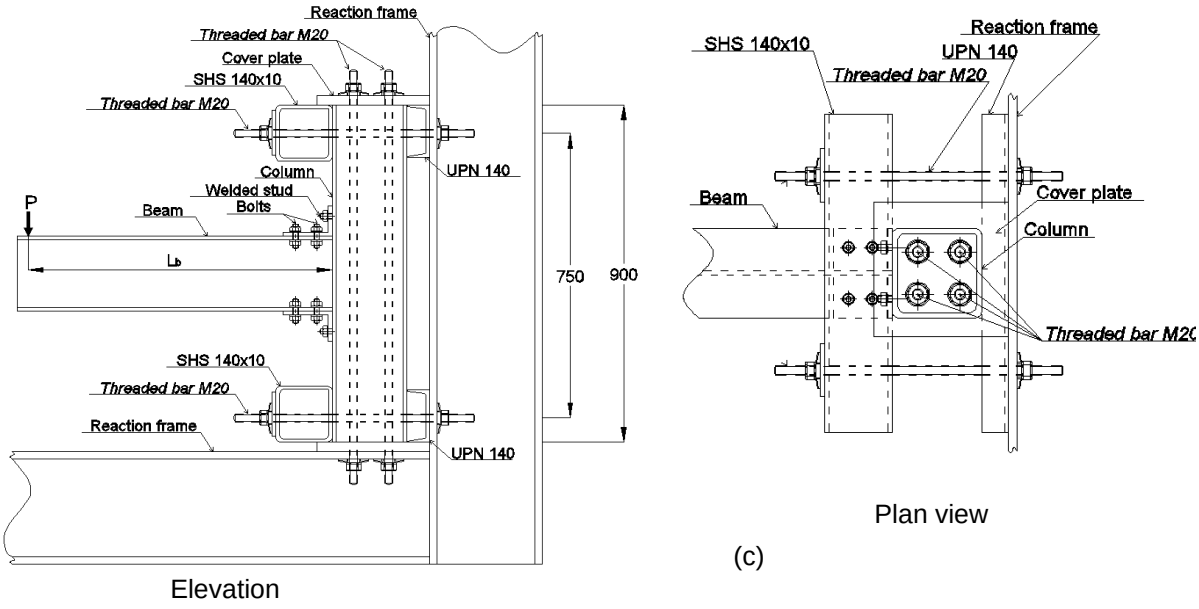

Figure 4. (a) Cyclic test on specimen SCS3. (b) External bracing system. (c) Sketch of the column restrain system, elevation and plane views

The Quasi-Static cyclic load protocol of [21], shown in Figure 5, was followed in this research. Table 2 lists the selected amplitudes together with the speeds of vertical displacement of the actuator. The amplitude increases by 40% from one step to the next until step 10 with an amplitude of 23.7 mm. Thereafter, the amplitude was increased by 30% from one to the next step. Two cycles of tension/compression load were applied for each amplitude of displacement. The test continued until failure occurred in the specimen.

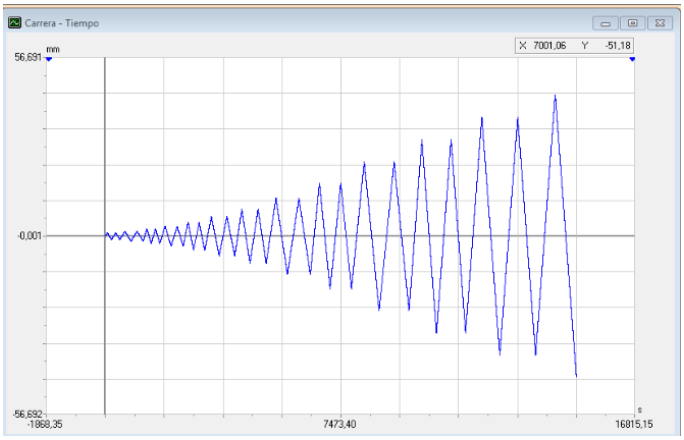

Figure 5. Displacement history in cyclic tests (according to [21])

Table 2: Amplitude of displacement and loading speed in cyclic tests

Δ [mm]	1.1	1.6	2.3	3.2	4.4	6.2	8.6	12.1	16.9	23.7	30.8	37.9	45.0
Speed [mm/min]	1	1	2	2	3	3	4	4	6	6	8	8	8

The jack displacement speed, starting at 1 mm/min in the first cycle and increasing to a maximum speed of 8 mm/min for the largest displacements, were selected to ensure an acceptably long duration of the test to facilitate observation and a manageable file size for DIC recording. The sampling frequency of the DIC system was nearly the same at each displacement ramp with a value of 0.1 Hz (image capture every 10 seconds). This resulted in test durations of longer than 4 hours with about 1500 captured images per test.

2.2. Beam-column joint specimen details

Six hollow sections (SHS200×6, SHS200×8, SHS200×10, RHS200×150×6, RHS200×150×8 and RHS200×150×10) as tubular columns and two open sections (HEB200 and IPE300) as beams, were used to make different beam-column joint specimens. The chosen sections are quite common in the construction of low to medium-rise buildings The dimensions of the angle cleats (120 ×80×10mm) were the same in all tests to keep uniformity of the joints but the angle cleats was not a critical factor in this research.

Two beam flange width to column width ratios (β) were considered to observe possible column failure modes (side wall failure or surface failure). The nominal steel grade for all tubes, beams and angles was S275 although their actual mechanical properties were determined by coupon tests. M16 Grade 8.8 for double sided joints and M16 Grade 10.9 bolts in case of single sided joints were used to connect the long leg of the angle cleats to the flanges of the beams. The bolts were pre-stressed with torques of 150 Nm and 250 Nm, applied in two steps, to the Grades 8.8 and 10.9 bolts respectively

The short legs of the angle cleats were bolted to the column face through the welded studs. The threaded studs were M16 Grade 4.8, M16 Grade K800 and M20 Grade 4.8 for the DMS, SMS and SCS series of joints, respectively. The lengths of the studs were 35mm in the specimens with double sided configuration and 40 mm in other tests. The nuts on the studs for the DMS and SMS joints were tightened by applying torques of 120 Nm and 190 Nm respectively. For the SCS joints whose threaded studs had a diameter of 20 mm but with a Grade of 4.8, a torque of 150 Nm was applied.

Table 1 presents a summary of the three test series including the column and beam sections, the β ratio (ratio of the beam flange width to the front face width of the column), the beam span (L_B in figures 3c and 4c) and the grades of bolts and threaded studs for every joint.

3. Test results

3.1. Mechanical properties of steel

The tensile coupons were cut from the walls of the six different tubes, from one flange (F) and the web (W) of the two beam sections and from the long leg (L) and the short leg (S) of the angle cleats. These coupons were tested following the standard tensile test procedure [22] until failure, in a universal testing machine (model MTS810) with a maximum load capacity of 100 kN. The tests were carried out under displacement control at a speed of 1mm/min. The DIC equipment with a 50mm focal length was used to measure the displacements of the coupons, which were used to determine the 0.2% proof stress, the ultimate tensile stress and the Young's Modulus of the specimens. Table 3 presents these results for the twelve tested coupons.

Table 3: Mechanical properties for tubes, beams and angle cleats

Column (h_0xb_0xt_0)	*f_y [N/mm^2]*	*f_u [N/mm^2]*	*E [Gpa]*
200x150x6	335.2	406.3	203.4
200x150x8	393.0	515.9	201.4
200x150x10	502.7	600.3	
200x200x6	377.2	476.1	215.3
200x200x8	411.4	483.4	
200x200x10	417.0	520.1	
Beam	*f_y [N/mm^2]*	*f_u [N/mm^2]*	*E [Gpa]*
HEB200 (F)	325.2	492.7	195.7
HEB200 (W)	334.9	482.0	192.3
IPE300 (F)	337.1	501.9	197.3
IPE300 (W)	350.5	499.0	213.6
Angle cleat 120x80x10	*f_y [N/mm^2]*	*f_u [N/mm^2]*	*E [Gpa]*
Short leg (S)	316.6	468.8	176.4
Long leg (L)	322.5	469.6	201.5

3.2. Mechanical properties of studs

A small number of coupon tests were carried out to determine the mechanical properties of the threaded welded studs used in the three series of beam-column joint tests according to table 1. Two coupons from each series of tests were prepared by machining them in the workshop to achieve a cylindrical shape and circular cross section, as shown in Figure 6(a), with diameters of 6.1 mm and 5.65 mm for specimens S16 and S20 and gauge lengths of 17 mm and 9.65 mm respectively. Specific threaded devices were used to attach the coupon ends to the grips of the testing machine (see figure 6 b-c). The coupons were tested in the same loading machine with a displacement rate of 1 mm/min up to around the 0.2% proof stress and 2 mm/min thereafter. The coupon test terminated when the stud broke, always occurring in the reduced cross section of the coupon accompanied with large elongation. The DIC equipment was also used in these tests to measure the displacements on the surface of the coupon, allowing to plot the stress-strain curves. Figure 7 presents a pair of samples of these curves for studs of grades K800 and 4.8 respectively.

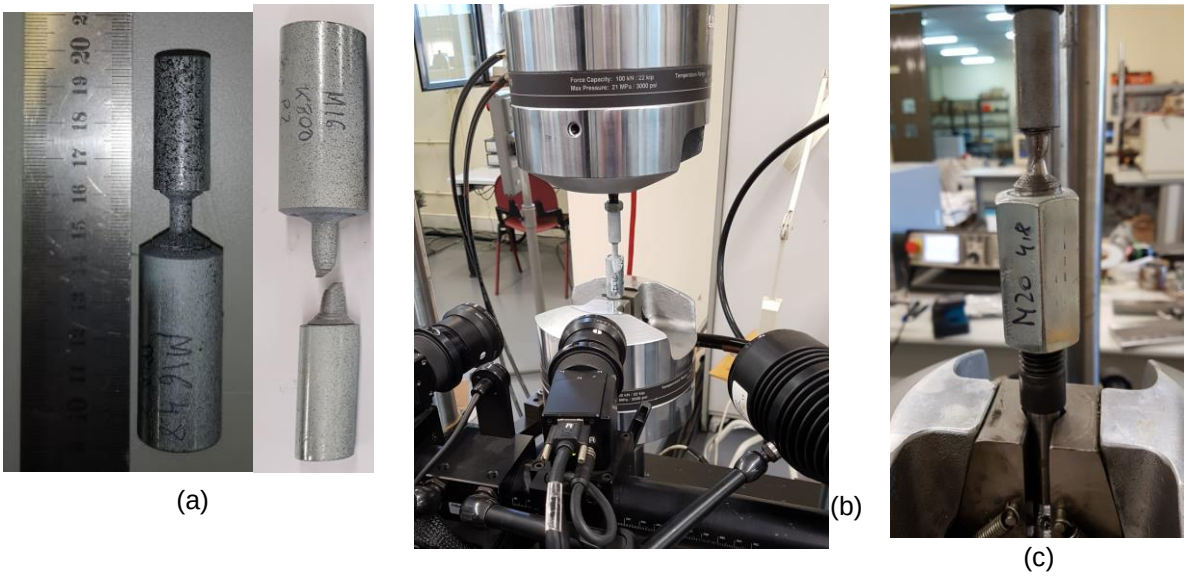

(a) (b) (c)

Figure 6. Tension tests on studs. (a) Coupon shape. (b) Test with DIC equipment. (c) Grips

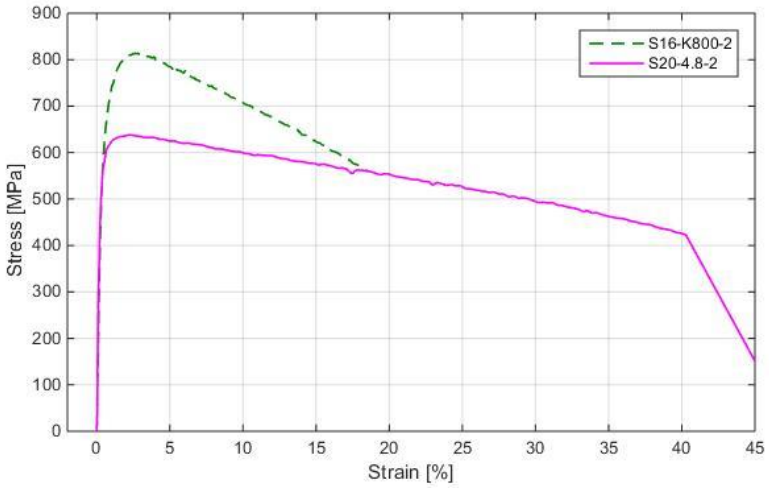

Figure 7. Typical stress-strain curves of Grade K800 and Grade 4.8 studs

Table 4 summarizes the obtained mechanical properties of studs, including the 0.2% proof stress (f_y), the ultimate tensile stress (f_u) and their ratio.

Table 4: Mechanical properties for threaded studs

Specimen	f_y [N/mm^2]	f_u [N/mm^2]	f_u/f_y
S16-4.8-1	455.22	493.74	1.08
S16-4.8-2	417.53	494.15	1.18
S16-K800-1	579.75	834.52	1.44
S16-K800-2	629.10	814.51	1.29
S20-4.8-1	573.49	638.42	1.11
S20-4.8-2	481.73	634.91	1.32

3.3. Monotonic test results

(a) Failure modes

Two main ultimate failure modes were observed in the beam-column joints: punching shear failure in the front face of the tube around the studs (figure 8a) and tension fracture of the

welded stud (figure 8 b). The threaded stud fracture was considered to be due to tension, not shear, due to necking of the studs. All the joints with a column thickness of 6 mm failed by punching shear while those with a column thickness of 10 mm failed by tension of the studs. In case of columns with a tube thickness of 8 mm, the type of failure was dependent on the stud diameter. The failure mode was tension of the studs in series DMS and SMS with a stud diameter of 16 mm and punching failure for series SCS that used studs of 20 mm in diameter.

Punching shear failure occurred after noticeable deformation in the front face of the tube, and this was more evident when the width ratio β was lower than one. Failure by tension of the studs, associated with thicker tubes or smaller studs, was accompanied by large deformation of the angle cleats. For the double-sided joints, where the shear force in the studs was relatively high due to short span of the beams and lower steel grade (4.8) of the studs which had lower resistance but were more ductile, there was a kind of combined failure mode of punching on the tube front face and tension fracture of the studs in case of thinner tubes of 6mm in thickness, as shown in figure 8c. Therefore, even with the afore-mentioned low bolt strength and high shear which could lead to stud failure in these four joints, the high ductility of the joint allowed extensive stress redistribution after initial cracking, with the ultimate failure mode being a combined failure mode.

Even though the beam web was not connected to the column, there was no shear failure of the beam or shear fracture of the threaded shear studs.

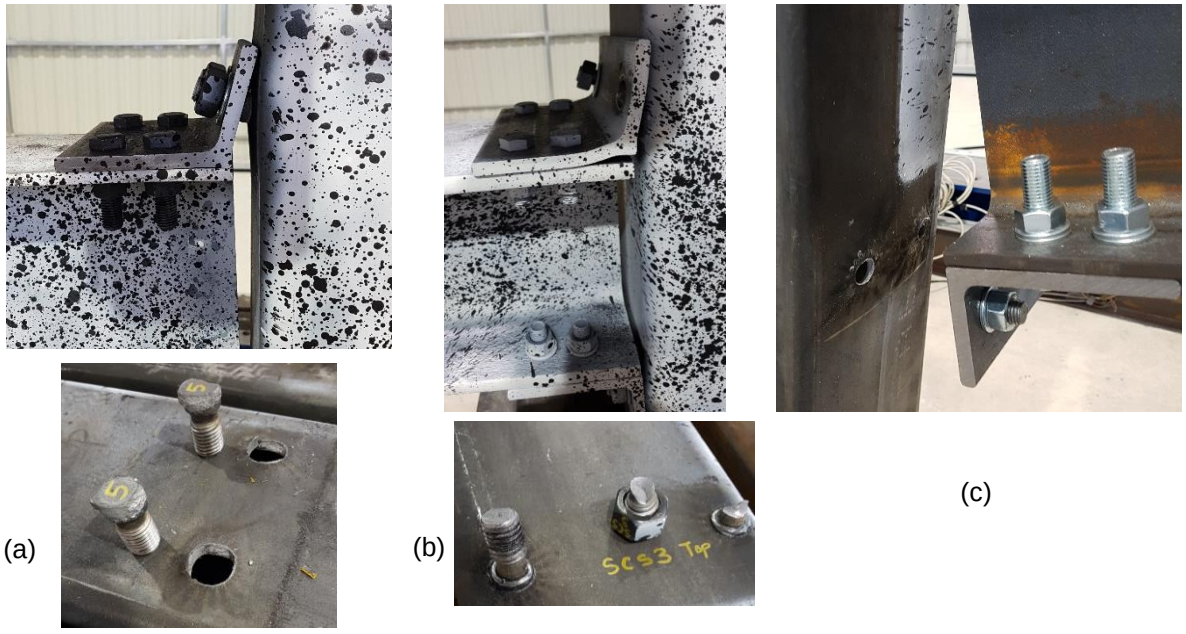

Figure 8. Failure modes. (a) Punching shear in SCS5, (b) Tension failure of welded stud in SCS3. (c) Combined punching and tension in DMS2

(b) Moment-rotation curves

Prior to loading, the data logger and the DIC device were synchronised so that the DIC images and recorded displacement were for the same load. The colours of DIC images indicate displacement and Figure 9 shows typical DIC images captured during the tests for joints DMS1 and SMS4 respectively.

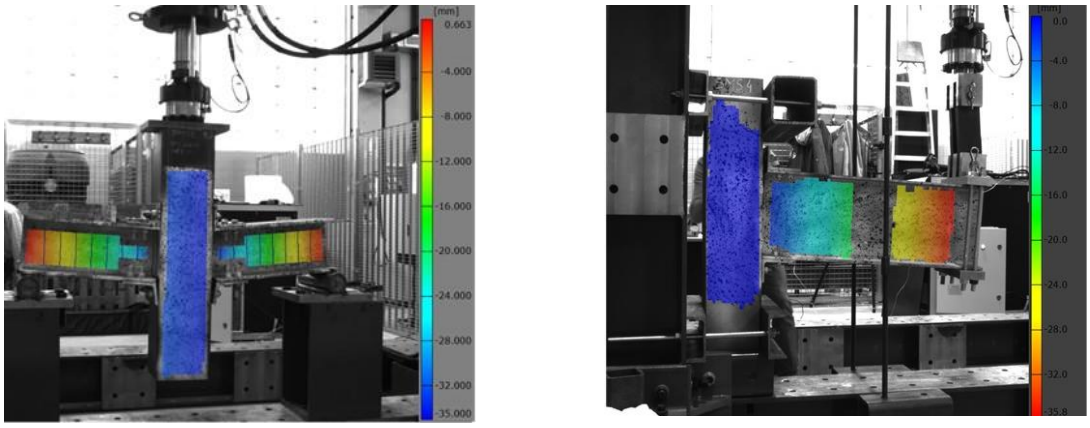

Figure 9: DIC images of displacement fields, (a) DMS1 and (b) SMS4

The DIC images, together with the recorded loads, were used to obtain the joint moment-rotation results. The span for calculating the joint bending moment was taken between the support and the front face of the tube (as presented in table 1 and shown in figure 3a) for DMS joints and from the actuator axis to the tube frontal face for SMS and SCS joints (as shown in figures 3c and 4c). The moment of the joint was calculated as the product of the introduced vertical load and the aforementioned span. The rotation of the joint was determined by the difference the displacements of the flanges under tension and compression divided by the depth of the beam.

Figure 10 shows an example of moment-rotation curves for one of the double sided joints, confirming symmetrical behaviour as intended. Therefore, in subsequent analyses, the average results of the two joints on the two sides of the column will be used for the double sided joints.

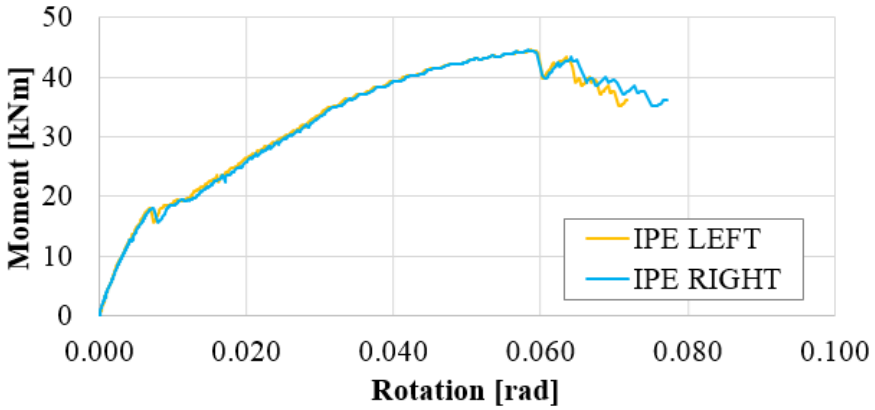

Figure 10: Moment rotation curves for left and right joints in specimen DMS1

Table 5 lists the calculated joint rotational stiffness and table 6 the bending moment at yield and at a rotation of 30 mrad for all the static loaded beam-column joints. The value of initial stiffness was obtained as the slope of the moment-rotation curve before 3 mrad since the curve is practically linear in all the tests until this rotational value. These values are compared with the boundary values for simple and rigid connections in non-sway construction according to EN 1993-1-8 [14] to for classifications of these joints. The ratios to rigid stiffness boundary are also included in table 5. To calculate the stiffness boundaries, a nominal beam span/depth ratio of 20 was used for the deep IPE beams or 30 times for the shallow HEB beams. According to the results in Table 5, all the joints behaved as semi-rigid with initial rotational stiffness values ranging from 13% to 43% of the stiffness for fully rigid joints with only two of the joints below 10%. As expected, the joint stiffness increased with increase of the tube wall thickness. Also, the joint stiffness was higher for beam-column joints with a width ratio of 1.0 when compared with similar joints with a lower width ratio. At β=1.0, the joint stiffness increases considerably being 55% to 88% of the value for similar joints with β=0.75 .

Table 5: Initial rotational stiffness S_{ini} [kNm/rad] of beam-column joints under static monotonic load. (In brackets the ratio to rigid stiffness boundary)

HEB200 (β=1.0)				IPE300 (β=0.75)					IPE300 (β=1.0)			
DMS1 t=8mm	SMS1 t=6mm	SMS2 t=8mm	SMS3 t=10mm	DMS2 t=6mm	DMS3 t=8mm	SMS4 t=6mm	SMS5 t=8mm	SMS6 t=10mm	DMS4 t=8mm	SMS7 t=6mm	SMS8 t=8mm	SMS9 t=10mm
2744	1973	2801	3671	1384	2882	2050	3795	4945	5924	3828	5886	9303
(18%)	(13%)	(18%)	(24%)	(7%)	(13%)	(10%)	(18%)	(23%)	(28%)	(18%)	(27%)	(43%)
Pinned connection: S=956				Pinned connection: S=1340								
Rigid connection: S=15303				Rigid connection: S=21445								

Table 6: Moment at yield [kNm] and at a rotation of 30 mrad of joints under static monotonic load

	HEB200 (β=1.0)				IPE300 (β=0.75)					IPE300 (β=1.0)			
	DMS1	SMS1	SMS2	SMS3	DMS2	DMS3	SMS4	SMS5	SMS6	DMS4	SMS7	SMS8	SMS9
M_{yield}	33.3	21.4	34.1	26.9	24.5	25.7	21.4	30.2	26.1	29.9	28.3	29.3	29.1
M_{30mrad}	33.5	21.6	-	-	27.6	37.9	28.1	38.9	-	56.9	36.2	-	-

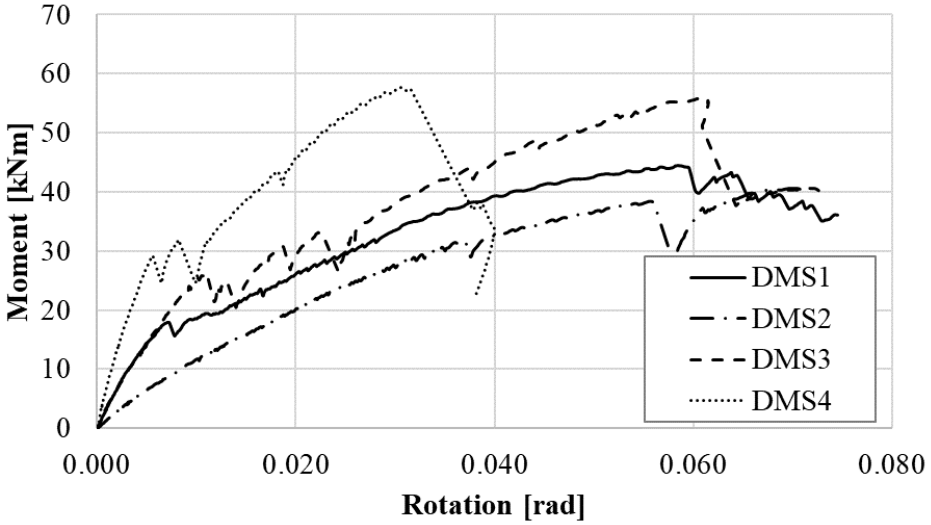

Figure 11: Moment rotation curves for joints DMS

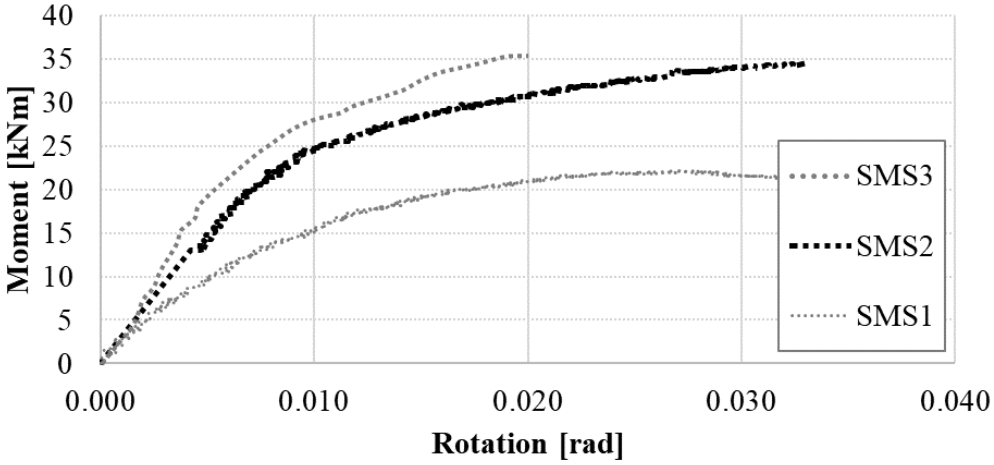

Figure 12: Moment rotation curves joints SMS1-3

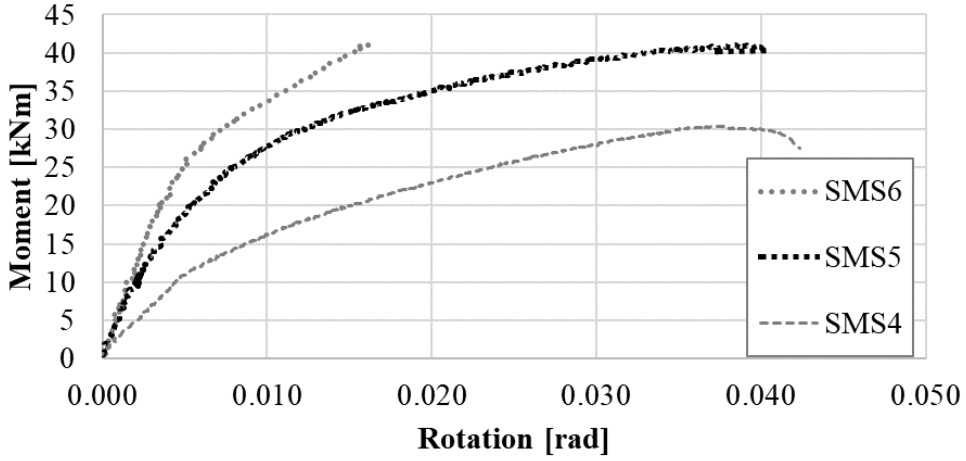

Figure 13: Moment rotation curves joints SMS4-6

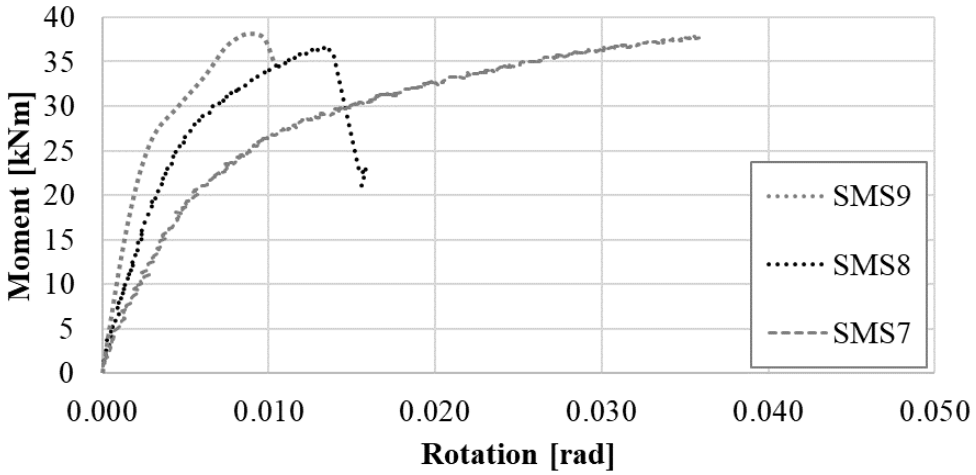

Figure 14: Moment rotation curves joints SMS7-9

Figures 11 to 14 show the complete moment rotation curves for all the monotonic tests, figure 11 being for double sided joints and figures 12 to 14 being for the single sided joints according to table 1. As expected the moment resistance increased with increase of the width ratio and the tube wall thickness Due to the failure mode, only minor differences were registered when comparing tubes of 8 mm and 10 mm in thickness. Most of joints achieved rotations greater than 0.03 rad which is typically considered to indicate ductile behaviour. Linearity of the moment-rotation curves to high moments can be observed and this was used to obtain reliable joint initial stiffness as the slope of the linear range. When single and double sided joints of the same dimensions are compared (e.g. comparison of figure 11 and figures 12 to 14) it can be seen that the rotation capacity was higher in case of double side specimens due mainly to higher ductility of the studs used for these joints (Grade 4.8 in double sided joints DMS, Grade K800 in single sided joint SCS, see their stress-strain curves in figure 7). Also joints of series SCS that included welded studs of grade 4.8 and were tested under cyclic loads, showed higher rotations as can be seen in their curves moment-rotation included in figure 15.

3.4. Cyclic tests

The same bending moment and rotation definitions as for the monotonic tests were adopted for the cyclic tests. Figure 15 shows individual hysteretic moment-rotation curves for every joint tested under cyclic load.

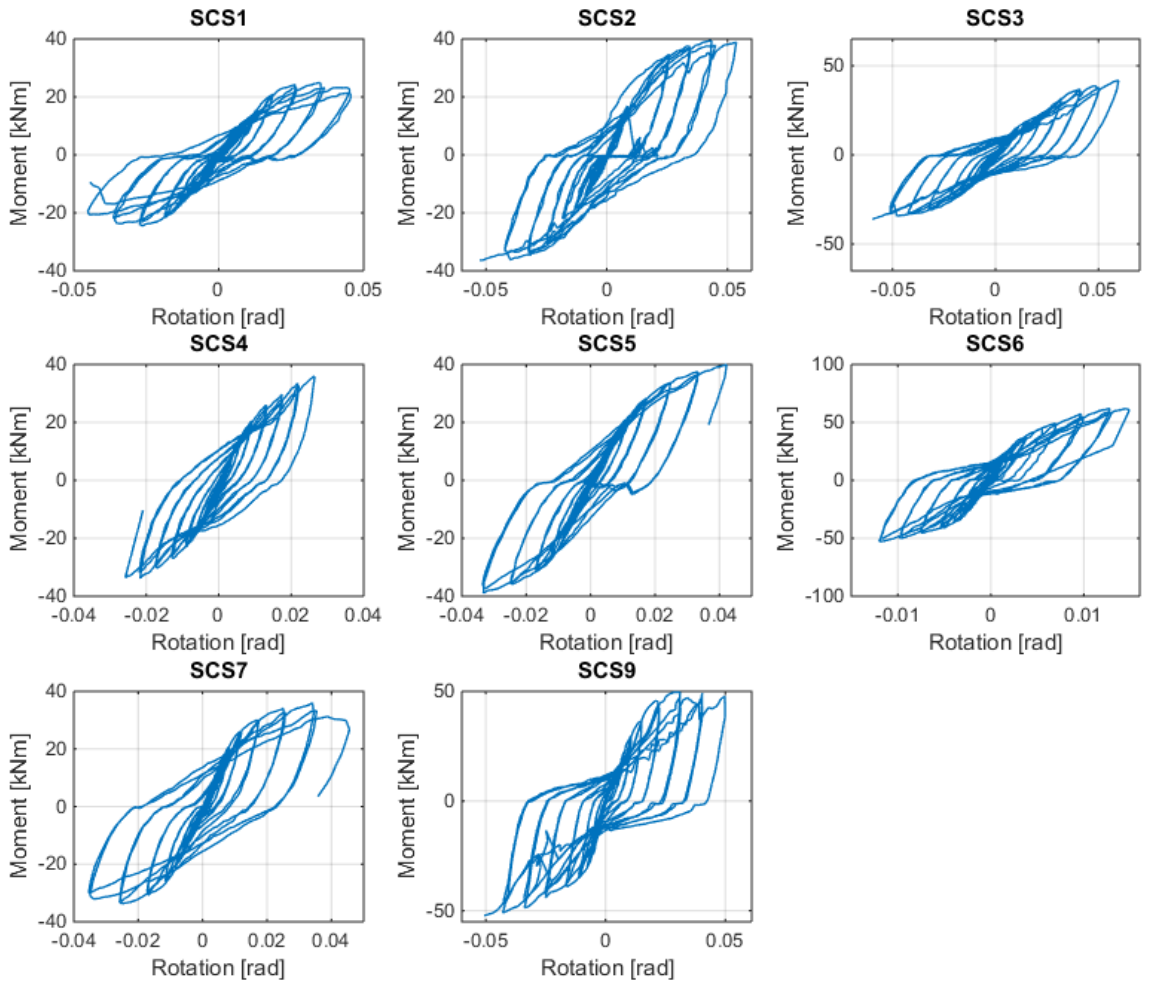

Figure 15. Hysteretic response of the specimens tested under cyclic load

These curves exhibit a small horizontal plateau during the transition from positive to negative bending moments. This behaviour is known as pinching [23] and it is due to the nuts of the studs experiencing a partial loss of the initial torque caused by the rough edge created around the studs during welding. This burr, introduced into the holes of the angle, would suffer a permanent deformation by the previous cyclic loading step (see figure 16). This process leads to the loss of some contact between the angle cleat and the column. The pinching behaviour is generally thought to be undesirable because of the resulting low hysteresis energy. In the opinion of the authors, this effect can be avoided by drilling a lightly higher diameter hole in the angle cleat or drilling a countersunk hole. The reloading branch was different for each cycle but in all cases reached practically the same peak load from which the previous cycle was unloaded. Furthermore, the unloading branches are largely parallel to each other regardless of the rotation magnitude.

Figure 16. Burring effect in the hole of the cleat

Table 7 lists the bending moment and the maximum rotation at yield for each of the cyclic loaded beam-column joints. Also the maximum rotation and ductility ratio defined as the maximum rotation to the rotation at yield [24] is presented in the table. The values of moment and rotation at yield were obtained from a bilinear idealization of the corresponding backbone curve for every joint.

Table 7: Moment and rotation at yield, maximum rotation and ductility ratio in cyclic tests

Specimen	Moment at yield [kNm]	Rotation at yield [mrad]	Max. rotation [mrad]	Max rotation / Rotation at yield
SCS1	23.807	20.41	44.50	2.18
SCS2	37.882	18.50	53.60	2.90
SCS3	32.109	22.69	59.70	2.63
SCS4	23.165	7.41	26.50	3.58
SCS5	30.212	14.51	42.20	2.91
SCS6	52.493	4.24	14.50	3.42
SCS7	27.953	10.68	38.70	3.62
SCS9	46.855	17.89	49.80	2.78

Figure 17 compares the cumulative dissipated energy *vs.* the cumulative rotation of all the tests. Table 8 summarizes the total energy dissipation values, the dissipated energy at a rotation of 1 rad and the rate of energy dissipation as the slope of curves from figure 17. As expected, joints with higher rotational stiffness were able to dissipate a higher energy rate.

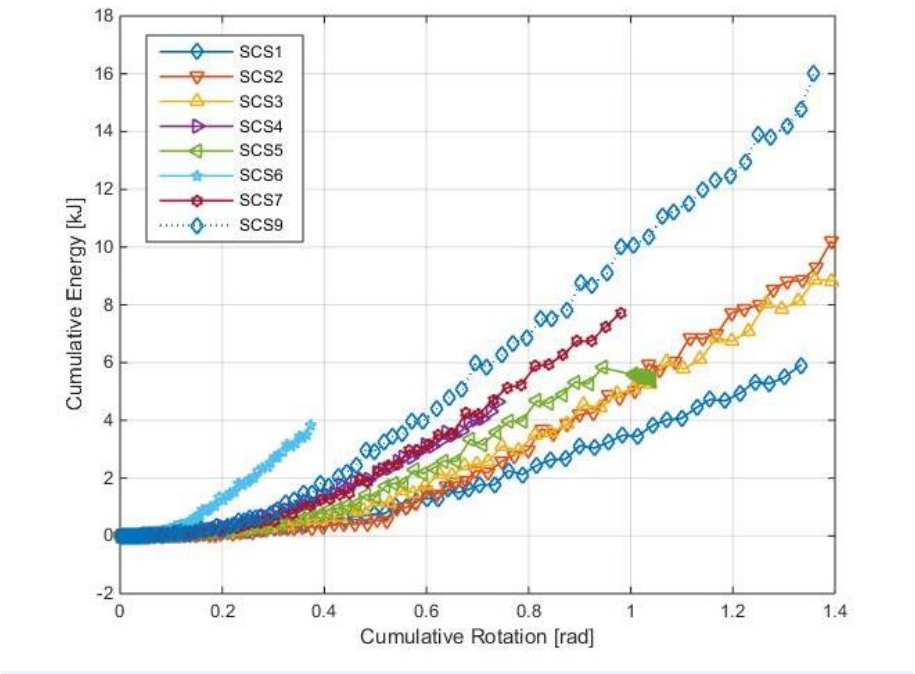

Figure 17. Cumulative energy dissipation

Table 8: Energy dissipation for specimens in cyclic tests

Specimen	Total energy dissipation [kJ]	Energy dissipation for rotation of 1 rad [kJ]	Rate of energy dissipation [kJ/rad]
SCS1	5.91	3.44	5.80
SCS2	13.91	4.9	10.59
SCS3	15.02	5.09	9.23
SCS4	4.6	-	7.87
SCS5	6.25	5.44	9.66
SCS6	-	11.79	13.50
SCS7	7.71	-	11.42
SCS9	17.14	10.06	14.15

The apparently low energy dissipation exhibited by specimen SCS6 (purple line in figure 17) was due to premature stop of the test by mistake, after hearing a strong noise during the test that seemed to indicate failure. The dissipation energy would have been considerably higher so the numerical value is not included in table 8.

Under cyclic loading, the dimensionless energy dissipation capacity $\bar{E}$ of the joint can be obtained as follows [25].

$$\bar{E} = E_{d,total}\frac{3 \cdot E \cdot I_b}{M_{pb}^2 \cdot L} \qquad (1)$$

where

$E_{d,total}$ is the total energy dissipation capacity of the joint;

E is the Modulus of elasticity of steel;

I_b is the second moment of inertia of the beam cross-section;

M_{pb} is the plastic bending moment resistance of the beam cross section and

L is the distance of the column front face to the point of load application

Table 9 presents the calculated results for the total dissipated energy and for the dissipated energy when the rotation of the joint is 1 rad. These results are similar to those (in Table 10) obtained by Elghazouli et al. [3] when using similar beam-column joint combinations but using blind bolts and angle cleats to connect beams and columns. Therefore, the proposed joint system of this research has a comparable dissipation capacity with the blind bolting system, but the proposed joint system is much easier to fabricate.

Table 9: Dimensionless energy dissipation capacity

Joint	Maximum rotation	Rotation: 1 rad
SCS1	8.60	5.01
SCS2	20.24	7.13
SCS3	21.85	7.41
SCS4	10.26	-
SCS5	13.95	12.14
SCS6	-	26.31
SCS7	17.20	-
SCS9	38.25	22.45

Table 10: Cumulative and dimensionless energy dissipation based on tests of [3]

Specimen	Cyclic Tests. Cumulative energy		Dimensionless energy dissipation capacity	
	Total energy [kJ]	Rotation of 1 rad [kJ]	Max [kJ/kJ]	1 rad [kJ/kJ]
A5.0-G8.8-d65-Y	6	4	10.15	6.77
A6.3-G8.8-d65-Y	8	5	13.54	8.46
A6.3-G8.8-d40-Y	12	7.4	20.31	12.52
A10-G8.8-d65-Y	11.5	7.3	19.46	12.35
A10-G10.9-d65-Y	12.5	7.5	21.15	12.69
C10-G10.9-d65-Y	25	15.5	24.33	15.08
C10-G10.9-d40-Y	30	19.5	29.19	18.97

4. An example case study

To demonstrate the benefits of using the propose system to achieve structural efficiency by taking advantage of semi-rigid, partial-strength behaviour of the proposed joints, and their suitability in moderate seismic regions, a case study has been performed on a three-bay, four-storey frame (figure 18) with typical design loads and spans. This structure represents an internal frame of a rectilinear residential building with the columns on a 5-meter square grid. For this illustrative structure, all the columns are RHS 200×150×8 with a fixed foundation and all the beams are IPE300. Cross bracings are included to prevent lateral displacements of the structure. The steel grade is S275. Table 11 lists the characteristic loads. A ground

acceleration of 0.12g corresponding to light to moderate potential damage in case of an earthquake, was considered. All the ultimate limit state calculations were made following Eurocode 3 EN 1993-1-1. The serviceability deflection limits were L/300 for the beams and H/500 for the columns. The beams were assumed to be laterally and torsionally restrained along the top flange only.

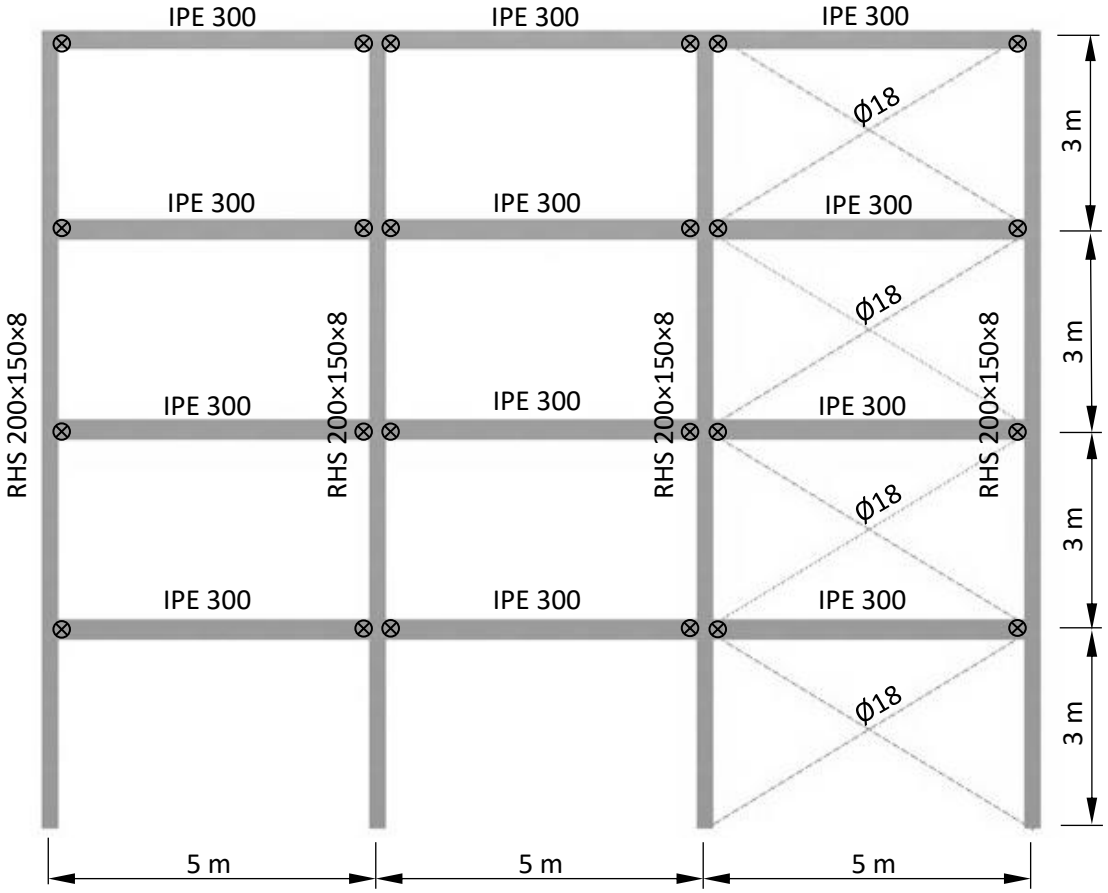

Figure 18. General view of the frame.

Table 11: Characteristic Loads [kN/m^2]

Type of load	Floors	Roof	Lateral
Dead load	4	4	-
Live load	2	1	-
Snow	0	1	-
Wind	-	-	+0.8; -0.4

This study compares the utilisation factors of the frame assuming pinned, semi-rigid and rigid connection behaviour. For semi-rigid design, the joint stiffnesses were taken as those obtained experimentally and reported in table 5 for DMS4 and SMS8. According to the EC3-1.8 [14] recommendations, 100% of these values were used for the serviceability limit state (SLS) calculations and 50% of these values for the ultimate limit state (ULS) calculations. This is

because the bending moments in the joints under SLS loads are below 2/3rd of the joint moment resistances, and those under ULS loads are more than 2/3rd of the joint resistances. Figure 19a compares bending moment diagrams of the frame with different joint types under SLS loads. Figure 19b compares the corresponding axial force diagrams with negligible differences.

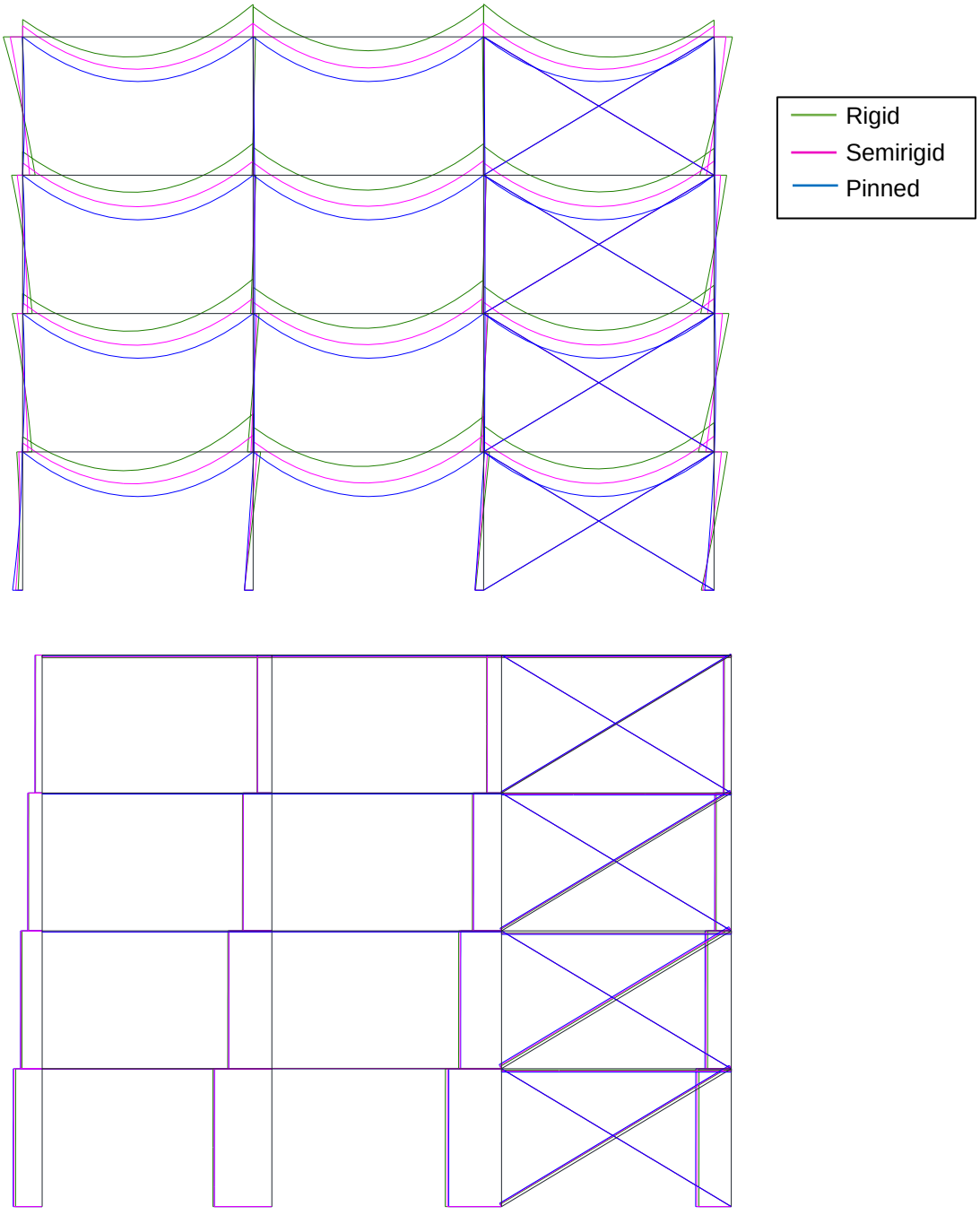

Figure 19. Internal forces diagrams with different joint types: (a) Bending moment (b) Axial force.

Figure 20 compares the utilisation factors for the frame assuming three different joint conditions. The utilisation factor is defined as highest ratio for resistance (applied force/ resistance) and for deflection (deflection/deflection limit).

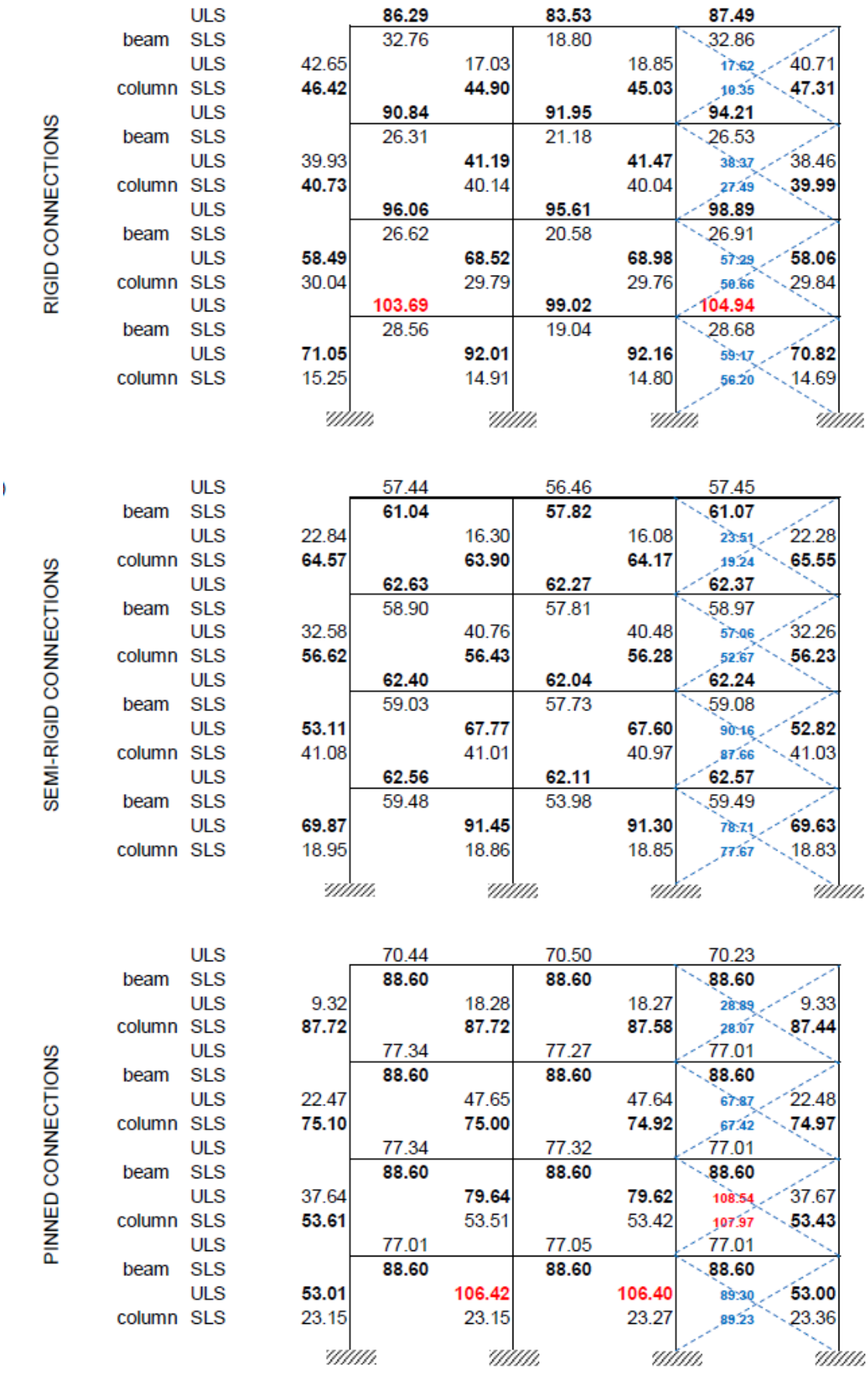

Figure 20. Utilization factors of beam and columns in ULS and SLS calculation for frames with rigid, semirigid and pinned beam-column joints (in %).

When using pinned connections, most of the lateral loads are resisted by the bracing system, and two of the braces were over loaded with an utilisation factor of more than 100% (108%). When the rotational stiffness of the joints was included in semi-rigid design, the lateral loads shared by the bracing were reduced and all the bracing members had utilisation factors less than 100%. On the other hand, when using fully rigid joints, two beams on the first floor would fail the design checks under ULS loads (utilisation rate 104%) caused by lateral torsional buckling of the unrestrained lower flange.

5. Conclusions and design recommendations

This paper has presented the results of an extensive experimental campaign to investigate the monotonic and cyclic moment-rotation behaviour of a new type joint between open steel beam to tubular steel column. The new joint system consists of angle cleats bolted to the beam flanges and bolted to the tube face via welded threaded steel stud. A total of 21 tests were carried out, including nine single sided and four double sided joints under monotonic loading and eight single sided joints under cyclic loading. These tests were designed to investigate the effects of changing beam size, changing column size and their width ratios. An example frame design was carried out to compare the performance of a plane frame assuming pinned joint behaviour, rigid joint behaviour, and joint behaviour obtained from the experiments. The following conclusions and design recommendations can be drawn.

1. The joint failure mode was either tensile fracture of the welded studs of bolt punching of the tube surface. Tensile fracture of stud happens when the tube wall thickness is high and the stud diameter or stud steel grade is low. To avoid punching failure, a minimum tube wall thickness of 8 mm is recommended.

2. The new joints behaved as semi-rigid and partial-strength joints according to EN 1993-1-8 definition with joint initial rotational stiffness values ranging from 13% to 43% of the stiffness for fully rigid joint (8EI/L). The joint stiffness increases with increased tube wall thickness and higher beam width to tube width ratio.

3. Frame design using the experimental joint behaviour can achieve advantages compared to assuming either pinned or rigid joint behaviour. The frame with pinned joint behaviour has higher utilisation factors in the bracing and in the beams. Whilst the frame with rigid joint behaviour may suffer premature failure in some beams due to lateral torsional bucking under hogging bending moment.

4. The new joints have a moderate level of energy dissipation capacity and can be used in moderate seismic zones.

5. The proposed joints are cheap, easy to execute, not requiring specialized manpower. They can be disassembled easily, allowing for reuse thus contributing to sustainable construction.

6. M20 bolts should be used. Grade K800 bolts should be avoided in order to achieve a reasonable amount of joint moment resistance and ductile behaviour of the studs.

Acknowledgements

The authors would like to acknowledge the financial support provided by the Spanish Ministry of Economy and Competitiveness through project BIA2017-83467-P, pre-doctoral grant PRE2018-084273 and by CIDECT through project 5CF. They would also like to thank the IEMES Research Group from the University of Oviedo for their support.

References

[1] Eekhout M, Tubular Structures in Architecture*,* CIDECT, Geneva and TU Delft. 2011.

[2] Wardenier J, Packer JA, Zhao XL and Van der Vegte GJ, Hollow Sections in Structural Applications. 2nd Edition, CIDECT, Switzerland, 2010.

[3] Elghazouli AY, Málaga-Chuquitaype C, Castro JM, Orton AH, Experimental monotonic and cyclic behaviour of blind-bolted angle connections, Engineering Structures, 31, 2540-2553. 2009.

[4] Thai HT and Uy B, Rotational stiffness and moment resistance of bolted end plate joints with hollow or CFST columns, Journal of Constructional Steel Research, 126, 139-152, 2016.

[5] Thai HT, Uy B, Yamesri, Aslani F, Behaviour of bolted end plate composite joints to square and circular CFST columns, Journal of Constructional Steel Research, 131, 68-82, 2017.

[6] Wang YC and Li X, Experimental study of moment-rotation characteristics of reverse channel connections to tubular columns, Journal of Constructional Steel Research, 85, 92-104, 2013.

[7] Málaga-Chuquitaype C and Elghazouli AY, Behaviour of combined channel/angle connections to tubular columns under monotonic and cyclic loading, Engineering Structures*,* 32, 1600-1616, 2010.

[8] Serrano-López MA, López-Colina C, Wang YC, Lozano M, Gayarre FL, Comparative behaviour of 'I beam- RHS column' joints with and without web weld, Journal of Constructional Steel Research, 159, 330-340, 2019.

[9] Maquoi R, Naveau X, Rondal J, Beam-Column Welded Stud Connections, Journal of Constructional Steel Research, 4, 3-26, 1984.

[10] Vandegans D, Use of Threaded Studs in Joints between I-Beam and RHS-Column, IABSE Reports, 75, 53-62, 1996.

[11] Tamboli AR, Handbook of Steel Connection design and Details. Mc Graw Hill, 2009.

[12] Davison B and Owens GW, Steel designers' manual. The Steel Construction Institute. Blackwell publishing, 2003.

[13] Weynand W, Jaspart JP, Steenhuis M, Economy Studies of Steel Building Frames with Semi-Rigid Joints, Journal of Constructional Steel Research*,* 46, (1-3) 85, 1998.

[14] Eurocode 3: Design of Steel Structures. Part 1-8: Design of Joints, EN-1993-1-8:2005, CEN. European Committee for Standardization, 2005.

[15] López-Colina C, Serrano-López MA, Gayarre FL, Suárez FJ, Resistance of the component `lateral faces of RHS' at high temperature, Engineering Structures, 32, 1133-1139, 2010.

[16] López-Colina C, Serrano MA, Lozano M, Gayarre FL, Suárez JM, Wilkinson T, Characterization of the main component of equal width welded I-beam-to-RHS-column connections, Steel and Composite Structures, 32-3, 337-346, 2019.

[17] Shim CS, Lee PG, Yoon TY, Static behavior of large stud shear connectors, Engineering Structures, 26-12, 1853-1860, 2004.

[18] Xue W, Ding M, Wang H, Luo Z, Static behavior and theoretical model of stud shear connectors, Journal of bridge engineering, 13-6, 623-634, 2008.

[19] Roberts TM and Dogan O, Fatigue of welded stud shear connectors in steel–concrete–steel sandwich beams, Journal of Constructional Steel Research, 45-3, 301-320, 1998.

[20] Johnson RP, Resistance of stud shear connectors to fatigue, Journal of Constructional Steel Research, 56-2, 101-116, 2000.

[21] FEMA 461: Interim Testing Protocols for Determining the Seismic Performance Characteristics of Structural and Nonstructural Components, Federal Emergency Management Agency, Washington, D.C., 2007.

[22] ASTM. Standard test methods for tension testing of metallic materials. ASTM E8/E8M: 2016, United States.

[23] Gusella F, Orlando M, Spinelli P, Pinching in steel rack joints: numerical modelling and effects on structural response, International Journal of Steel Structures 19-1, 131-146, 2019.

[24] Ye J, Mojtabaei SM, Hajirasouliha I, Seismic performance of cold-formed steel bolted moment connections with bolting friction-slip mechanism, Journal of Constructional Steel Research 156, 122-136, 2019.

[25] Yang JG, Kim YB, Kwak MS, Evaluation of the energy dissipation capacities of beam-to-column moment connections for steel frames, Journal of Asian Architecture and Building Engineering, 15-3, 573-579, 2016.